Chemical Physics Letters 691 (2018) 211–218

Contents lists available at ScienceDirect

Chemical Physics Letters

journal homepage: www.elsevier.com/locate/cplett

Research paper

Synthesis and structural characterization of ZnO-and CuO-NPs supported mesoporous silica materials (hexagonal SBA-15 and lamellar-SiO_2)

Issa M. El-Nahhal [a,*], Jamil K. Salem [a], Nihal S. Tabasi [a], Rolf Hempelmann [b], Fawzi S. Kodeh [a]

[a] Department of Chemistry, Al-Azhar University, P.O. Box 1277, Gaza, Palestine
[b] Physical Chemistry, Saarland University, 66123 Saarbrucken, Germany

ARTICLE INFO

Article history:
Received 16 September 2017
In final form 14 November 2017

Keywords:
Hexagonal and lamellar-SiO_2 structures
ZnO&CuO-NPs supported mesoporous silica
Mesoporous silica
Pluronic surfactants
ZnO&CuO-NPs

ABSTRACT

Two different mesoporous silica structures (hexagonal and lamellar) were synthesized via sol-gel method using a series of triblock copolymer (Pluronic) surfactants. L81, L61 & L31 surfactants form lamellar structure whereas P123 surfactant forms a hexagonal structure. CuO and ZnO nanoparticles (NPs) supported mesoporous silica were synthesized using impregnation method. The structural properties of these materials were investigated using several characterization techniques such as FTIR, XRD, SAXS, TEM and TGA. SAXS and TEM confirmed that the obtained mesoporous silica is based on the EO/PO ratio of Pluronic surfactants. They proved that the mesoporosity of silica is well maintained even after they loaded with metal oxide nanoparticles.

1. Introduction

Metal oxide nanoparticles exhibit unique physical and chemical properties due to their limited size and a high surface area to volume ratio [1]. Metal oxides are especially attractive with respect to applications in catalysis [2], sensing [3], energy storage [4] and biomedical application [5]. During last years, the interest of mesoporous silica materials has increased due to the great benefits that these materials can offer. Mesoporous silica materials, discovered in 1992 by the Mobile Oil Corporation, have received considerable attention due to their superior textual properties such as high surface area, large pore volume, tunable pore diameter, and narrow pore size distribution [6–8]. Because of their utilities in drug delivery systems, adsorption, selective separation and catalysis, mesoporous silica materials are highly desirable for various purposes and applications [9–12]. A variety of mesostructured materials exhibiting lamellar, hexagonal (*p6mm*), 3D hexagonal (P63/mmc) or cubic (*Ia3d*, *Im3m* and *Pm3n*) organizations have already been prepared under different preparative conditions [13,14]. Many types of ionic and non-ionic surfactants have been used for obtaining mesoporous silica with different pore structure and morphological characteristics [15]. The main surfactants used in the synthesis of mesoporous are non-ionic block copolymers. Advantages with block copolymers are their stability to time the ordering by varying solvent composition, molecular weight or copolymer composition [16]. The length of the EO chains is essential for establishing the mesoporous structure. Polymers with short EO chains form lamellar structures; with medium length chains, two-dimensional hexagonal structures are preferentially formed; and long EO chains favor a cubic structure [13,14,17,18]. Incorporation of metal oxide nanoparticles in mesoporous silica materials has been a very interesting and promising field of research such as catalysis [19], optics [20] and drug delivery [21]. Some of the methods used for modification mesoporous silica are direct synthesis [22,23] and post modification like impregnation [24–26]. There are a number of different Pluronics available, with a selection of different molecular weights and variations in the EO/PO ratio. The tendency for $(EO)_x$-$(PO)_y$-$(EO)_x$ block copolymers to adopt different structures depending on temperature and their composition (EO/PO ratio). The length of PO block has more relation with pore size and silica order [16], while the length of the EO chains is essential for establishing the mesoporous structure [13,14,17,18]. The effect of different block lengths of triblock copolymers in the formation of mesoporous silica has been studied for a series of Pluronic surfactant (L101, P103, P104, P105, F108, P65, P84 and P123) [13,14,17]. The main objective of our present research, is

* Corresponding author.
E-mail address: issanahhal@alazhar.edu.ps (I.M. El-Nahhal).

https://doi.org/10.1016/j.cplett.2017.11.030
0009-2614/

that mesoporous silica of hexagonal or lamellar structure materials are prepared based on EO/PO ratio and the length of EO chain using a series of nonionic triblock copolymer surfactants (Pluronic P123, L81, L61 and L31). The prepared mesoporous silica using nonionic triblock copolymers surfactants (Pluronic L81, L61 and L31) are found to produce lamellar silica structure, whereas the use of P123 surfactant is found to produced hexagonal mesoporous silica. The series has similar short length of EO block, but only they have different length of PO block. Therefore their corresponding mesoporous silica have general lamellar structure with minor differences. In case of using P123 surfactant which has medium length EO block produced a hexagonal mesoporous silica structure. Obviously the formation of different mesoporous structures is refer to the difference of hydrophilicity and hydrophobicity properties of the used surfactants [14]. The two types of mesoporous silica structures (hexagonal and lamellar) have a different behavior towards the incorporation of metal oxides. The systematic procedure for synthesis of mesoporous silica and their supported metal oxides (CuO, and ZnO) via impregnation method are presented in Scheme 1. Several methods and techniques are used to examine their structural properties. These methods include fourier transform infrared spectroscopy (FTIR), X-ray diffraction (XRD), small angle X- ray scattering (SAXS), transmission electron microscopy (TEM) and thermal gravimetric analysis (TGA),

2. Experimental

2.1. Materials

All the chemicals used were analytical grade and directly used as received without further purification. Triblock copolymer Pluronic L31 (EO_2 PO_{16} EO_2, 99%), Pluronic L61 (EO_2 PO_{31} EO_2, 99%), Pluronic L81 (EO_3 PO_{43} EO_3, 99%), Pluronic P123 (EO_{20} PO_{70} EO_{20}), Tetraethoxyorthosilicate (TEOS) ($Si(OC_2H_5)_4$) and copper acetate monohydrate ($Cu(CH_3COO)_2{\cdot}H_2O$) were purchased from Aldrich company. Zinc acetate dihydrate ($Zn(CH_3COO)_2{\cdot}2H_2O$) was purchased from Sigma Company. Hydrochloric acid (HCl, 37%) was purchased from Merck Company. All the glassware used in this experimental work washed with distilled water and dried at 100 °C.

2.2. Synthesis of mesoporous silica

In a typical synthesis of mesoporous silica [13], 4.0 g of nonionic triblock copolymer Pluronic surfactant (P123, L81, L61, and L31) was dispersed in 40 mL of deionized water under stirring for 1 h. The solution of each surfactant (L81, L61 and L31) was kept at 10 °C. Then 60 mL of 2 M HCl was slowly added to the surfactant solution under the same conditions for another hour. TEOS (8.8 mL, 39.4 mmol) was added to previous mixture drop wise under the same conditions. The mixture was put under stirring at room temperature for 24 h. The mixture was autoclaved at 100 °C for 48 h. The product was filtrated, washed twice with 25 mL deionized water, and then dried at 100 °C for 24 h. The materials were calcinated at 600 °C for 3 h. The synthesized materials are labeled SiO_2-P123 (SBA-15), SiO_2-L81, SiO_2-L61, and SiO_2-L31, respectively.

2.3. Synthesis of supported metal oxides/mesoporous silica

Metal oxides (CuO and ZnO) nanoparticles supported mesoporous silica materials were prepared using impregnation method [25,26], by adding the desired amount (30%) of the appropriate metal acetate salts in deionized water to 0.7 g of each mesoporous silica. The mixture was stirred for 2 h at room temperature, and then was heated to 80 °C under stirring to dryness. The final product was dried at 100 °C overnight. The material was calcinated at 600 °C for 4 h. The obtained materials were labeled as CuO/SiO_2-P123 (SBA-15), CuO/SiO_2-L81, CuO/SiO_2-L61, CuO/SiO_2-L31, ZnO/SiO_2-P123 (SBA-15), ZnO/SiO_2-L81, ZnO/SiO_2-L61 and ZnO/SiO_2-L31.

2.4. Methodology

Infrared spectra for the materials were recorded on a Perkin-Elmer FTIR spectrometer using KBr disk in the range 4000–400 cm^{-1}. Thermogravimetric analysis (TGA) was carried out using Mettler Toledo TGA/SDTA851e analyzer in the range of 25–600 °C of heat rate of 10 °C/min. The system was purged with nitrogen using a flow rate of 50 mL/min. Powder X-ray diffraction (XRD) patterns were recorded on Analytical Expert Pro diffractometer utilizing Cu Kα radiation (k = 1.54 Å). The TEM analysis was

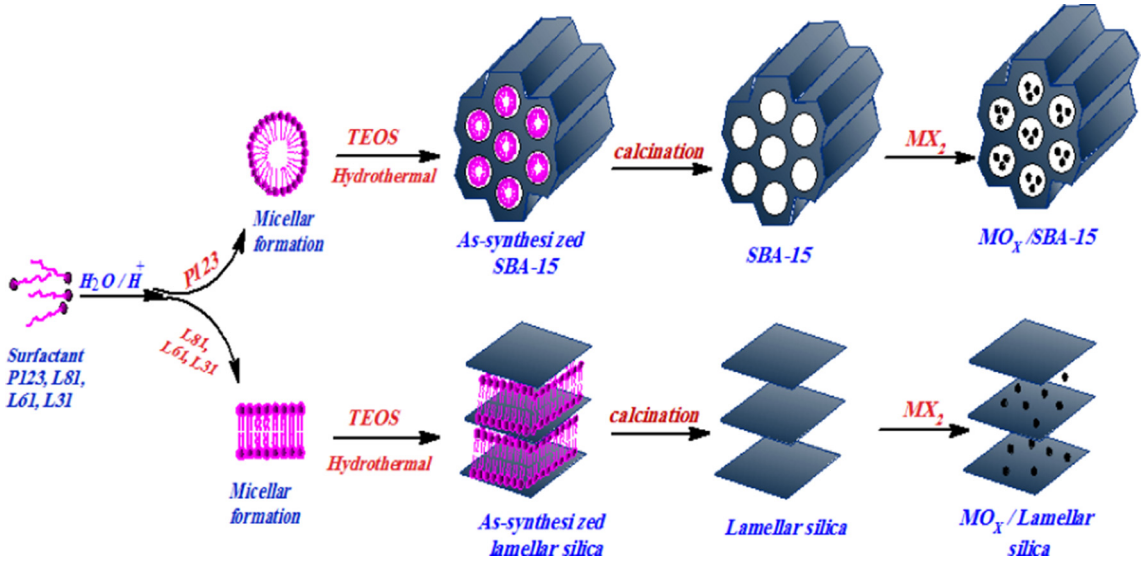

Scheme 1. Description of synthesis of supported metal oxide-mesoporous silica via impregnationmethod.

performed with JEM2010 (JEOL) transmission electron microscope with energy-dispersive X-ray spectrometer INCA (Oxford Instruments).

3. Result and discussion

3.1. Synthesis

Mesoporous silica was prepared using four different surfactants (L81, L61, L31 and P123) (Scheme 1). P123 copolymer surfactant form rod-like micelle to obtained well-ordered hexagonal structure. Copolymer surfactants (L81, L61, and L31) are probably formed different micelle shape of lamellar structures because of the short chain EO block copolymers of Pluronic surfactants. The silica obtained using Pluronic L81, L61, and L31 do not form a well pore-order as that of SiO_2-P123 (SBA-15). This was confirmed by SAXS analysis discussed later.

The complete removal of surfactant via thermal decomposition was observed for samples heated at 600 °C. Thus the lamellar structure was expected to collapse at high temperature at 600 °C. Apparently, the removal of the surfactant from 2D hexagonal structure did not produce any major change in the shrinkage behavior of retained its hexagonal, open pore structure even after heating at 600 °C [27]. However, the structural stability should be different from that of simple lamellar.

CuO- and ZnO-NPs supported mesoporous silica (30%) were prepared using post synthesis (impregnation) method [25,26]. In this method, mesoporous silica materials were treated with metal precursor solution. Metal precursor was loaded into/onto silica and then metal precursor was decomposed by thermal treatment as shown in Scheme 1. Using this method, there was a possibility of loaded the metal oxide nanoparticles into/onto mesoporous silica. This may leads to the formation of uncontrolled agglomerations of metal oxide onto the outer surface of mesoporous silica.

3.2. Fourier transform infrared (FTIR)

FTIR spectra of SiO_2-P123 (SBA-15) and SiO_2-L81 are generally similar (Fig. 1). However, there were some changes in the relative intensities of the peaks of OH and Si—O vibrations. The OH vibrations of the lamellar structure materials are higher than that of Si—O vibrations of hexagonal structure. This means that in lamellar materials are less stable with less cross-linking and collapsed at high temperature in comparison with hexagonal structure material. The spectra for both materials show same absorption peaks in the three functional regions at 3600–3400 cm^{-1}, 1700–1500 cm^{-1} and 1400–400 cm^{-1} correspond to ν(O—H), δ(O—H) and ν (Si—O—Si) vibrations, respectively. The FTIR spectra of SiO_2-P123 (SBA-15), CuO/SiO_2-P123 (SBA-15) and ZnO/SiO_2-P123 (SBA-15) materials are given in Fig. 2(a–c). A broad band in range of 3600–3400 cm^{-1} in Fig. 2(a–c) is due to ν(O—H) vibration. This is attributed to hydrogen-bonded between adsorbed water and MO and silica surfaces. The weak peak at 1645 cm^{-1} (Fig. 2(a–c)) is probably due to δ(O—H) vibrational [28]. A strong broad band around 1150–1000 cm^{-1} centered at 1085 cm^{-1} (Fig. 2(a–c)) is due to the asymmetric stretching vibrational of ν(Si—O) of silica network. The peak at 965 cm^{-1} (weak shoulder) in Fig. 2a is due to δ(Si—O) vibration of non-condensed silanol groups. The peak around 800 cm^{-1} (Fig. 2(a–c)) is due to symmetric stretching of Si—O—Si vibration from silica network. The peak around 459 cm^{-1} (Fig. 2(a–c)) is due to δ (Si—O) bending vibration from silica network [28,29]. The presence of a shoulder at about 560 cm^{-1}in Fig. 2(b&c) is related to (M—O) vibration for supported MO/mesoporous silica. There is no presence of absorption peaks related to surfactant, which gives a clear evidence that Pluronic surfactants are totally removed upon calcination.

FTIR spectra of SiO_2-P123 (SBA-15) (Fig. 2a) and MO/SiO_2-P123 (SBA-15) (Fig. 2(b&c)) are very similar, which give a good evidence about the physical interaction between MO and silica network.

3.3. X- ray diffraction (XRD)

XRD patterns of SiO_2-P123 (SBA-15), SiO_2-L81, SiO_2-L61 and SiO_2-L31 are given in Fig. 3(a–d). All mesoporous silica materials exhibit broad diffuse peaks at 2θ of ca. 23° which is attributed to the non-crystalline silica [28,30]. XRD patterns of SiO_2-L81, SiO_2-L61 and SiO_2-L31 (Fig. 3(b–d)) are similar to the XRD pattern of SiO_2-P123 (SBA-15) (Fig. 3a). This confirmed the amorphous nature of the synthesized mesoporous silica materials (SiO_2-L81, SiO_2-L61 and SiO_2-L31).

The XRD patterns of ZnO/SiO_2-P123 (SBA-15), ZnO/SiO_2-L81, ZnO/SiO_2-L61 and ZnO/SiO_2-L31 are shown in Fig. 4(a–d). All diffraction peaks of XRD matched with hexagonal phase (wurtzite structure) of ZnO (JCPDS card No. 89-7102) [31]. The major peaks at 2θ values of 31.7°, 34.35°, 36.17°, 47.46 °, 56.57°, 62.82°, 66.36 °, 67.9° and 69.04°can be indexed to the lattice planes of (1 0 0), (0 0 2), (1 0 1), (1 0 2), (1 1 0), (1 0 3), (2 0 0), (2 0 1) and (1 1 2) reflections, respectively [31–33]. The absence of any diffraction peaks related to impurities in XRD patterns may confirm high purity of the synthesized materials.

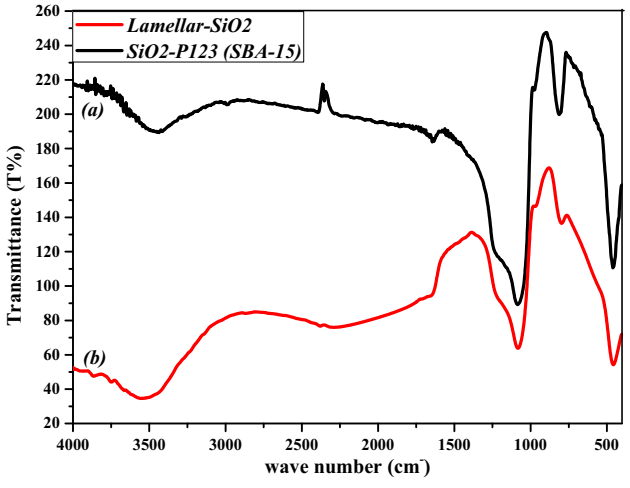

Fig. 1. FTIR spectra of (a) SiO_2-P123 (SBA-15) and (b) Lamellar-SiO_2.

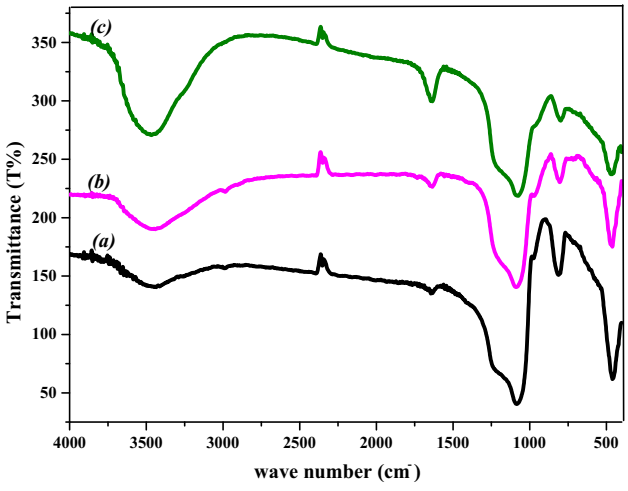

Fig. 2. FTIR spectra of (a) SiO_2-P123 (SBA-15), (b) CuO/SiO_2-P123 (SBA-15) and (c) ZnO/SiO_2-P123 (SBA-15).

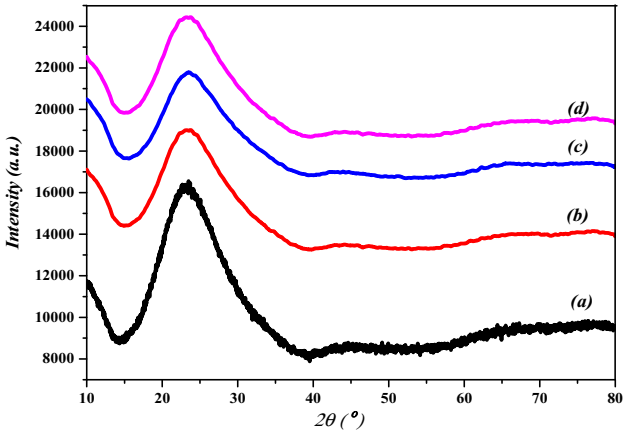

Fig. 3. XRD patterns of (a) SiO_2-P123 (SBA-15), (b) SiO_2-L81, (c) SiO_2-L61 and (d) SiO_2-L31.

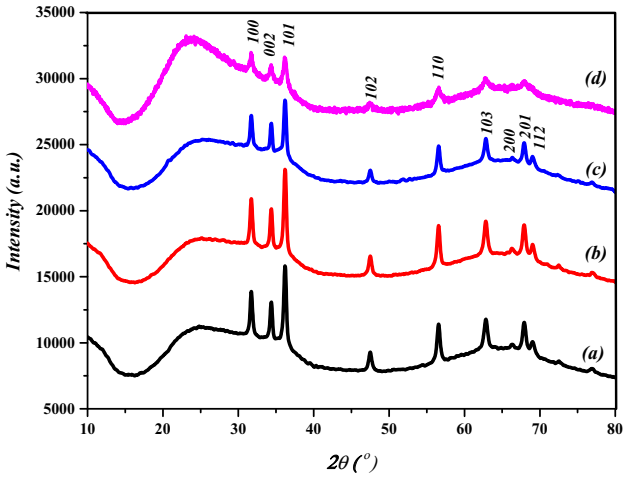

Fig. 4. XRD pattern of (a) ZnO/SiO_2-L81, (b) ZnO/SiO_2-L61, (c) ZnO/SiO_2-L31 and (d) ZnO/SiO_2-P123 (SBA-15).

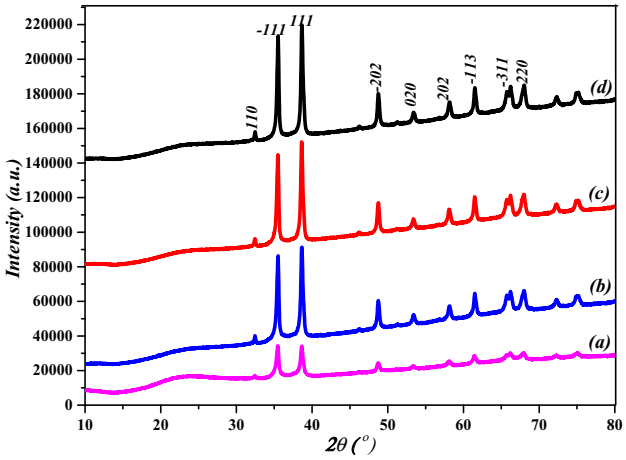

Fig. 5. XRD pattern of (a) CuO/SiO_2-P123 (SBA-15), (b) CuO/SiO_2-L31, (c) CuO/SiO_2-L61 and (d) CuO/SiO_2-L81.

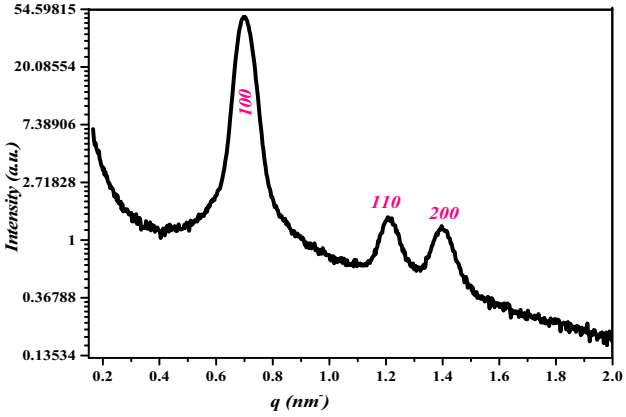

Fig. 6. SAXS results for SiO_2-P123 (SBA-15).

ZnO diffraction peaks in SiO_2-L81, SiO_2-L61 and SiO_2-L31 were more intense than in SiO_2-P123 (SBA-15). The reason for this behavior is that in the case of SiO_2-P123 (SBA-15), less ZnO nanoparticles are inserted into mesopores of the silica. That confirmed in the TGA section that discussed latter.

The XRD patterns of CuO/SiO_2-P123 (SBA-15), CuO/SiO_2-L31, CuO/SiO_2-L61 and CuO/SiO_2-L81 are presented in Fig. 5(a–d), respectively. All the peaks in the diffraction pattern indicate to the monoclinic phase of CuO, which is in good consistent with (JCPDS No. 05-0661) [34]. Diffraction peaks related to impurities were not found in XRD patterns, which confirm high purity of synthesized materials. The obvious main peaks correspond to the lattice planes of (1 1 0), (−1 1 1), (1 1 1), (−2 0 2), (0 2 0), (2 0 2), (−1 1 3), (−3 1 1), (2 2 0) [34,35]. CuO diffraction peaks in SiO_2-L81, SiO_2-L61 and SiO_2-L31 were more intense than in SiO_2-P123 (SBA-15). The low intensity peaks for CuO/SiO_2-P123 (SBA-15) is probably due to low content of CuO particles is loaded inside the pores in comparison with that of other mesoporous silica materials.

3.4. Small angle X-ray scattering (SAXS)

SAXS pattern of SiO_2-P123 (SBA-15) synthesized with Pluronic P123 (EO_{20} PO_{70} EO_{20}) surfactant depicts in Fig. 6. It shows a typical pattern of a hexagonal structure with the occurrence of a strong peak, due to the (1 0 0) plane, and other two weak peaks, due to the (1 1 0) and (2 0 0) planes. The presence of three well-resolved diffraction peaks is associated with highly ordered mesoporous silica SiO_2-P123 (SBA-15) with a two-dimensional hexagonal structure (space group *p6mm*) [28,36]. The d_{100} spacing value is 8.8 nm for silica SiO_2-P123 (SBA-15) and pore-to-pore distance (a_0) is 10.2 nm.

SAXS patterns of SiO_2-L81, SiO_2-L61 and SiO_2-L31 are given in Fig. 7(a–c). For SiO_2-L81, two broad peaks at q = 0.625 nm^{-1} and 3.25 nm^{-1}can be indexed as (0 0 1) and (0 0 2) reflections of lamellar structure [37,38]. There is a little variation in SAXS pattern between the SiO_2-L81 and those of SiO_2-L61 and SiO_2-L31. Although, they showed a typical pattern of lamellar structure similar to that of SiO_2-L81 with the occurrence of a broad peak at q = 3.25 nm^{-1}, due to (0 0 2) reflection of lamellar structure [14,39]. The difference between PO/EO ratios of the three surfactants (L81, L61 and L31) in comparison with that of P123 Pluronic surfactant is the main reason for the difference between the structures of the materials.

Fig. 8(a–c) showed SAXS patterns of SiO_2-L81 and its supported metal oxide ZnO/SiO_2-L81 and CuO/SiO_2-L81, respectively. SAXS patterns of CuO/SiO_2-L81 and ZnO/SiO_2-L81 (Fig. 8(b&c)) showed two well-resolved peaks indexed as (0 0 1) and (0 0 2) reflections were corresponded to lamellar structure as identical to that of SiO_2-L81 (Fig. 8a). This indicates that the insertion of ZnO or CuO nanoparticles with a controlled amount into the mesoporous silica

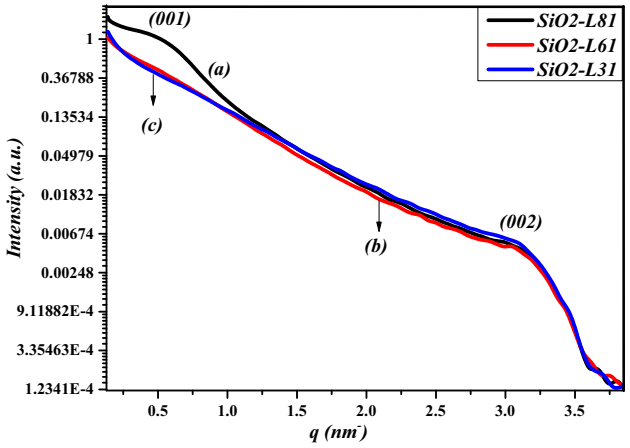

Fig. 7. SAXS results for SiO_2-L81.

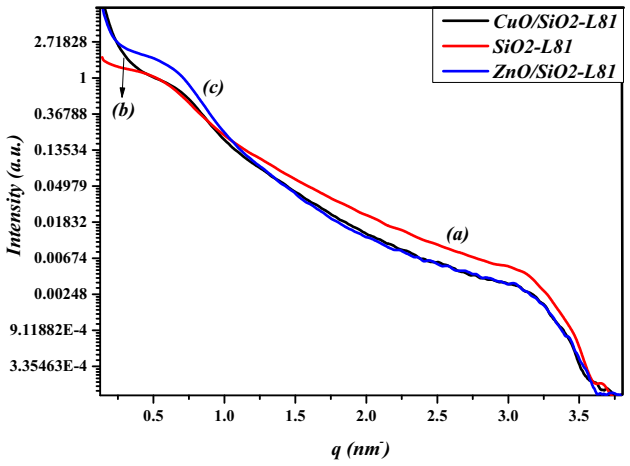

Fig. 8. SAXS pattern of (a) SiO_2-L81, (b) CuO/SiO_2-L81 and (c) ZnO/SiO_2-L81.

system does not obviously change the lamellar structure of SiO_2-L81 [22,40], but it improve the mesoporosity of the silica precursor (Fig. 8b).

Fig. 9(a–c) showed SAXS patterns of SiO_2-P123 (SBA-15) and their supported metal oxides CuO/SiO_2-P123 (SBA-15) and

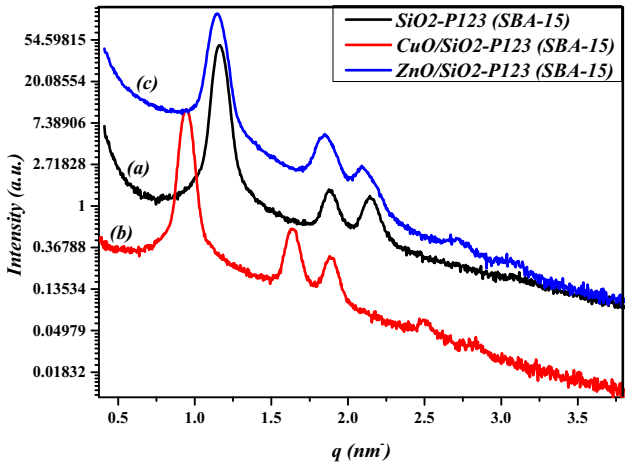

Fig. 9. SAXS pattern of (a) SiO_2-P123 (SBA-15), (b) CuO/SiO_2-P123 (SBA-15) and (c) ZnO/SiO_2-P123 (SBA-15).

ZnO/SiO_2-P123 (SBA-15), respectively. SAXS patterns of CuO/SiO_2-P123 (SBA-15) and ZnO/SiO_2-P123 (SBA-15) (Fig. 9 (b&c)) are similar to the pattern of SiO_2-P123 (SBA-15) (Fig. 9a). It showed a typical pattern of a hexagonal phase with the occurrence of a strong peak, due to the (1 0 0) plane, and other two weak peaks, due to the (1 1 0) and (2 0 0) planes. This provides evidence that the addition of inorganic precursors maintains the mesoscopic order of SiO_2-P123 (SBA-15) silica. There was a shift of all three peaks to a small q value after impregnation process. This result of increasing the inter-planar spacing, this suggest that the insertion of metal oxides CuO and ZnO is probably associated with expansion of the mesoporous silica [41]. Since the insertion of metal oxide precursors does not alter the peaks position in case of lamellar-SiO2 silica in comparison with that of SiO2-P123 hexagonal structure, the metal oxides are probably adsorbed onto the outside surface of lamellar silica.

3.5. Transmission electron microscopy (TEM)

TEM image of SiO_2-P123 (SBA-15), SiO_2-L81, CuO/SiO_2-L81 and ZnO/SiO_2-L81 materials are shown in Fig. 10(a–e). Fig. 10a shows the hexagonal arrangement of the pores, confirming the mesoporous hexagonal structure of SiO_2-P123 (SBA-15) material [17]. The estimated pore diameter is about 5.1 nm, center-to-center pore distance is about 10.2 nm which is exactly of same value obtained from SAXS analysis. TEM image of SiO_2-L81 (Fig. 10b) shows a wormhole-like mesoporous silica structure with no pore order as that of SiO_2-P123 (SBA-15). The high resolution image of SiO_2-L81 (Fig. 10c) shows an overlap of layers confirming the presence of lamellar structure of SiO_2-L81, which is in a good agreement with SAXS results [38]. Fig. 10d shows TEM image of ZnO/SiO_2-L81, the ZnO nanoparticles are seen in dark particles inserted into the pores of silica grey color. High-resolution image of ZnO/SiO_2-L81 (Fig. 10e) shows a clear pattern of channels where well crystalline ZnO-NPs are probably absorbed into the pores of silica. Low resolution of TEM image of CuO/SiO_2-L81 (Fig. 10f), the CuO nanoparticles are impregnated into the pores of SiO_2-L81. The High-resolution image of CuO/SiO_2-L81 (Fig. 10g) shows CuO-NPs in black color are covered the layers of silica. TEM images of supported metal oxides of SiO_2-P123 (SBA-15) are well established [22,40], so we are limited to report TEM analysis of ZnO/SiO_2-L81 and CuO/SiO_2-L81.

3.6. Thermal gravimetric analysis (TGA)

Thermal gravimetric analysis (TGA) and differential thermogravimetric analysis (DTA) for SiO_2-L81, SiO_2-P123 (SBA-15) and their supported metal oxides are examined under nitrogen at 25–600 °C at rate 10 °C/min (Figs. 11 and 12). The thermogram of the SiO_2-P123 (SBA-15) (Fig. 11a) shows twosteps of weightloss. The first step occurs at 75 °C due to loss of 1.2% of its initial weight. This is attributed to loss of physisorbed water from the system pores. The second step occurs at 300 °C due to loss of 1%, which is probably due to the condensation reaction of Si—OH groups. The total loss is 2.2% [42].Fig. 11b shows the thermogram of CuO/SiO_2-P123 (SBA-15), where two steps of weight losswere shown. The first step occurs 80 °C is due to 3.0% weight loss, which is attributedto loss of adsorbed H_2O on the surface of CuO-NPs and silica pores. The second step occurs over wide range at 200–600 °C is due to 2.2% weight loss, which is correspond to dehydroxylation of silanol and formation of siloxane bonds [34,42]. The total weight loss is 5.2%. The thermogram of ZnO/SiO_2-P123 (SBA-15) (Fig. 11c) shows a similar thermogram as that of ZnO/SiO_2-P123 (SBA-15). It shows two steps of weight loss. The first step occurs at 80 °C is due to 2.5% weight loss, which is attributed to loss of adsorbed H_2O on the surface of metal and silica pores. The second step occurs at

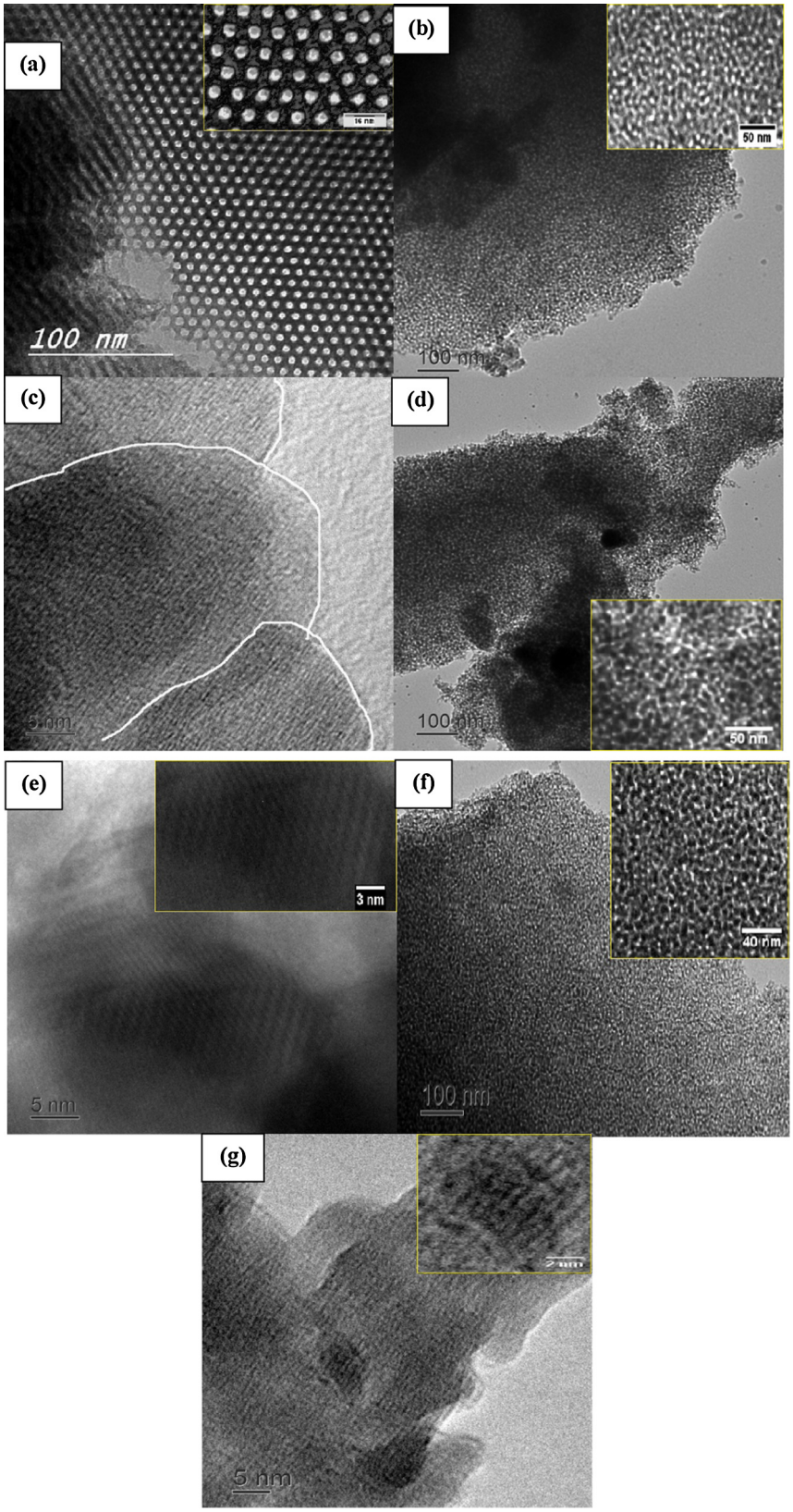

Fig. 10. TEM image of (a) SiO_2-P123 (SBA-15), (b) (low-resolution) SiO_2-L81, (c) (high-resolution) SiO_2-L81, (d) (low-resolution) ZnO/SiO_2-L81, (e) (high-resolution) ZnO/SiO_2-L81, (f) (low-resolution) CuO/SiO_2-L81 and (g) (high-resolution) CuO/SiO_2-L81.

wide range 200–600 °C due to 3.5% weight loss, which is correspond to dehydroxylation of silanol and formation of siloxane bonds [42–44]. The total loss is about 6.0% of initial weight.

Similarly, the thermogram of the SiO_2-L81 materials (Fig. 12a) shows twosteps of weight loss, the first step occurs at 75 °C due to loss of 1.4% of its initial weight. This is attributed to loss of

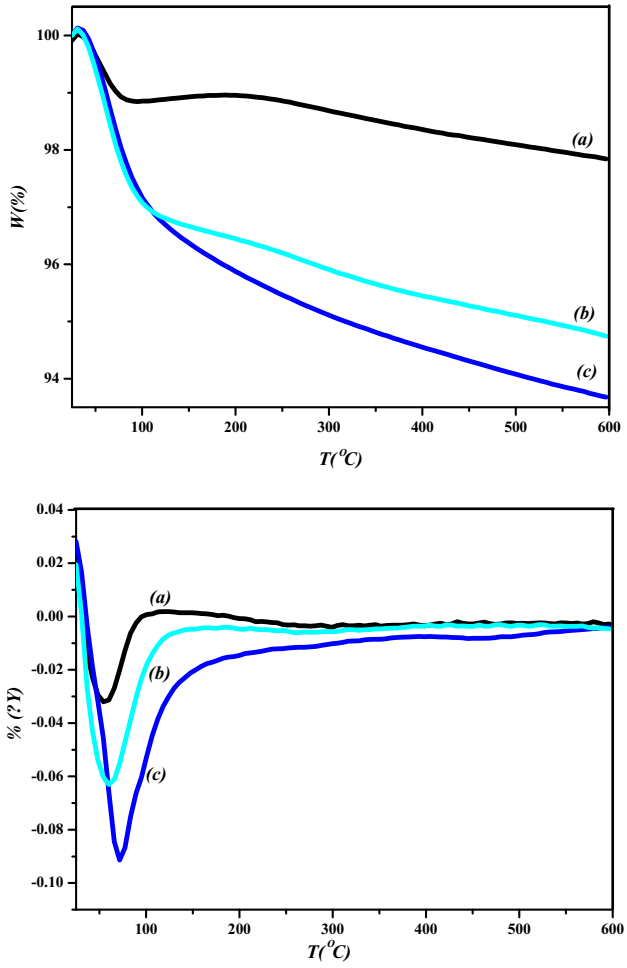

Fig. 11. TGA and DTA patterns of (a) SiO_2-P123 (SBA-15), (b) CuO/SiO_2-P123 (SBA-15) and (c) ZnO/SiO_2-P123 (SBA-15).

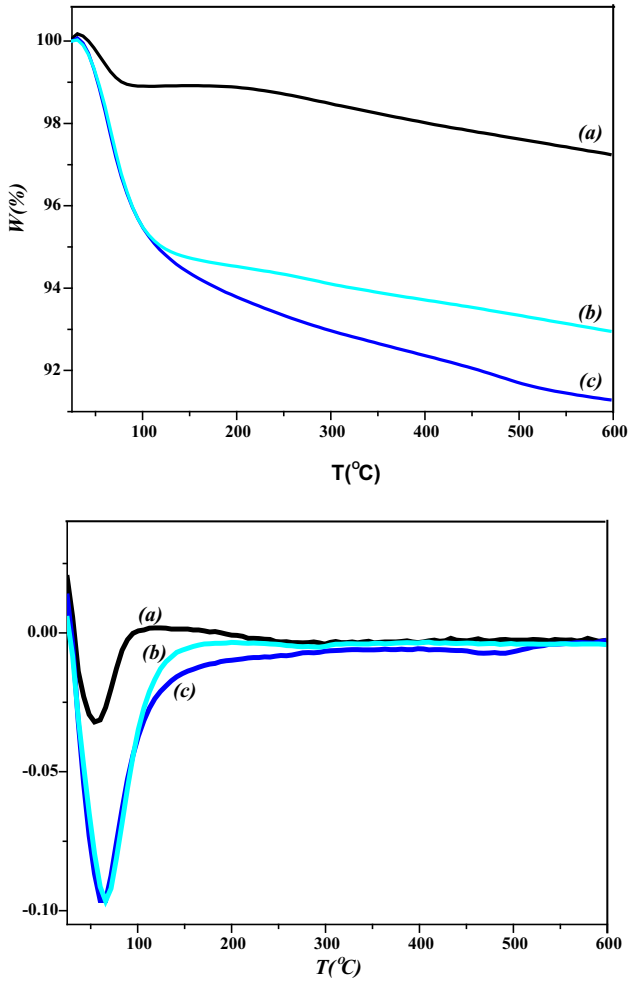

Fig. 12. TGA and DTA pattern of (a) SiO_2-L81, (b) CuO/SiO_2-L81 and (c) ZnO/SiO_2-L81.

physisorbed water from the system pores. The second step occurs at 300 °C due to loss of 1.2%, which is probably due to the condensation reaction between the Si—OH groups. The total loss is 2.6% [38].Fig. 12b shows the thermogram of CuO/SiO_2-L81, where two steps of weight loss were shown. The first step occurs 80 °C is due to 5.0% weight loss, which is attributed to loss of adsorbed H_2O on the surface of copper oxide nanoparticles and silica pores. The second step occurs over wide range at 200–600 °C is due to 2.1% weight loss, which is corresponded to dehydroxylation of silanol and formation of siloxane bonds [30,38]. The total weight loss is 7.1%. The thermogram of ZnO/SiO_2-L81 (Fig. 12c) shows two steps of weight loss. The first step occurs at 75 °C due to 5.5% weight loss, which is attributed to loss of physisorbed water on the surface of metal and silica pores. The second step occurs at 300–600 °C is due to 3% weight loss, which correspond to dehydroxylation of silanol and formation of siloxane bonds [38,39,40]. The total weight loss is 8.5%.

The difference in the weight loss in the first step between the silica and the encapsulated ZnO nanoparticles refers to the presence of crystallize water molecules of the zinc oxide. It seems that more ZnO or CuO nanoparticles absorbed onto SiO_2-L81 than SiO_2-P123 (SBA-15) silica.

4. Conclusion

Mesoporous silica materials (hexagonal- and lamellar-SiO_2) were synthesized using a series of triblock copolymer (Pluronic) nonionic surfactants (P123, L81, L61 and L31) as template by sol-gel method. Metal oxides nanoparticles (CuO and ZnO) were supported into/onto mesoporous silica by impregnation method. These materials were investigated by several characterization techniques, such as FTIR, XRD, SAXS, TEM and TGA. XRD analysis showed that mesoporous silica materials were in amorphous form. It is found from SAXS and TEM analysis that short EO chain surfactants (L81, L61 and L31) gives lamellar mesoporous structure, while medium EO chain surfactant (P123) gives 2D hexagonal (*P6mm*) mesoporous structure. SAXS and TEM confirmed that the introduction of CuO and ZnO metal oxides occurred onto/into mesoporous silica and they did not alter the mesoscopic structure. SAXS also suggested that the insertion of CuO and ZnO is associated with expansion of the SiO_2-P123 (SBA-15) silica network, whereas no change occurs in the case of lamellar-SiO_2 silica. TEM showed that all metal oxides were in crystalline form, monoclinic CuO and wurtzite ZnO.

Acknowledgements

We would like to thank Al Azhar University of Gaza for its generous financial support throughout the course of this research.

References

[1] K. Pathakoti, M.J. Huang, J.D. Watts, X. He, H.M. Hwang, J. Photochem. Photobiol. B 130 (2014) 234.

[2] A.A. Refaat, Int. J. Environ. Sci. Tech. 8 (2011) 203.
[3] Y.F. Sun, S.B. Liu, F.L. Meng, J.Y. Liu, Z. Jin, L.T. Kong, J.H. Liu, Sensors 12 (2012) 2610.
[4] J. Jiang, Y. Li, J. Liu, X. Huang, C. Yuan, X.W.D. Lou, Adv. Mater. 24 (2012) 5166.
[5] A.K. Gupta, M. Gupta, Biomaterials 26 (2005) 3995.
[6] F. Hoffmann, M. Cornelius, J. Morell, M. Fröba, Angew. Chem. Int. Ed. 45 (2006) 3216.
[7] P. Feng, X. Bu, D.J. Pine, Langmuir 16 (2000) 5304.
[8] C.T. Kresge, M.E. Leonowicz, W.J. Roth, J.C. Vartuli, J.S. Beck, Nature 359 (1992) 710.
[9] I.I. Slowing, J.L. Vivero-Escoto, C.W. Wu, V.S.Y. Lin, Adv. Drug Deliv. Rev. 60 (2008) 1278.
[10] L. Wu, H. Wang, H. Lan, H. Liu, J. Qu, Sep. Purif. Technol. 117 (2013) 118.
[11] É. Prouzet, C. Boissière, C. R. Chim. 8 (2005) 579.
[12] A. Taguchi, F. Schüth, Micropor. Mesopor. Mater. 77 (2005) 1.
[13] D. Zhao, Q. Huo, J. Feng, B.F. Chmelka, G.D. Stucky, J. Am. Chem. Soc. 120 (1998) 6024.
[14] P. Kipkemboi, A. Fogden, V. Alfredsson, K. Flodström, Langmuir 17 (2001) 5398.
[15] L.F. Giraldo, B.L. López, L. Pérez, S. Urrego, L. Sierra, M. Mesa, Macromol. Symp. 258 (2007) 129.
[16] A. Barrabino, Chalmers University of Technology, 2011.
[17] K. Flodström, V. Alfredsson, Micropor. Mesopor. Mater. 59 (2003) 167.
[18] D. Zhao, J. Feng, Q. Huo, N. Melosh, G.H. Fredrickson, B.F. Chmelka, G.D. Stucky, Science 279 (1998) 548.
[19] D. Barreca, W.J. Blau, G.M. Croke, F.A. Deeney, F.C. Dillon, J.D. Holmes, E. Tondello, Micropor. Mesopor. Mater. 103 (2007) 142.
[20] V. Hornebecq, M. Antonietti, T. Cardinal, M. Treguer-Delapierre, Chem. Mater. 15 (2003) 1993.
[21] Z. Li, J.C. Barnes, A. Bosoy, J.F. Stoddart, J.I. Zink, Chem. Soc. Rev. 41 (2012) 2590.
[22] Y.M. Wang, Z.Y. Wu, Y.L. Wei, J.H. Zhu, Micropor. Mesopor. Mater. 84 (2005) 127.
[23] H.S. Lee, W.H. Kim, J.H. Lee, D.J. Choi, Y.K. Jeong, J.H. Chang, J. Solid State Chem. 185 (2012) 89.
[24] J. Roggenbuck, T. Waitz, M. Tiemann, Micropor. Mesopor. Mater. 113 (2008) 575.
[25] A.M. Furtado, Y. Wang, T.G. Glover, M.D. LeVan, Micropor. Mesopor. Mater. 142 (2011) 730.
[26] J. Lee, J.H. Chang, J. Solid State Chem. 188 (2012) 100.
[27] T. Benamor, L. Michelin, B. Lebeau, C. Marichal, Micropor. Mesopor. Mater. 147 (2012) 334.
[28] H. Wanyika, E. Gatebe, P. Kioni, Z. Tang, Y. Gao, Afr. J. Pharm. Pharmacol. 5 (2011) 2402.
[29] Y. Li, N. Sun, L. Li, N. Zhao, F. Xiao, W. Wei, Y. Sun, W. Huang, Materials 6 (2013) 981.
[30] Q. Wang, B.Z. Li, Y. Li, Chin. Chem. Lett. 25 (2014) 253.
[31] D. Kundu, C. Hazra, A. Chatterjee, A. Chaudhari, S. Mishra, J. Photochem. Photobiol. B 140 (2014) 194.
[32] N. Talebian, S.M. Amininezhad, M. Doudi, J. Photochem. Photobiol. B 120 (2013) 66.
[33] T. İpeksaç, F. Kaya, C. Kaya, Mater. Lett. 100 (2013) 11.
[34] I.M. El-Nahhal, J.K. Salem, S. Kuhn, T. Hammad, R. Hempelmann, S. Al Bhaisi, J. Sol-Gel Sci. Technol. 1 (2016).
[35] C. Dong, X. Xiao, G. Chen, H. Guan, Y. Wang, Appl. Surf. Sci. 349 (2015) 844.
[36] J.P. Thielemann, F. Girgsdies, R. Schlögl, C. Hess, Beilstein J. Nanotechnol. 2 (2011) 110.
[37] J. García-Martínez, P. Brugarolas, S. Domínguez-Domínguez, Micropor. Mesopor. Mater. 100 (2007) 63.
[38] E. Dovgolevsky, S. Kirmayer, E. Lakin, Y. Yang, C.J. Brinker, G.L. Frey, J. Mater. Chem. 18 (2008) 423.
[39] X. Zhang, M. Tsapatsis, Micropor. Mesopor. Mater. 138 (2011) 239.
[40] Q. Lu, Z. Wang, J. Li, P. Wang, X. Ye, Nanoscale Res. Lett. 4 (2009) 646.
[41] I.M. El-Nahhal, J.K. Salem, M. Selmane, F.S. Kodeh, H.A. Ebtihan, Chem. Phys. Lett. 667 (2017) 165.
[42] D. Zhang, J. Li, Chin. Sci. Bull. 58 (2013) 879.
[43] I.M. El-Nahhal, J.K. Salem, S. Kuhn, T. Hammad, R. Hempelmann, S. Al Bhaisi, Powder Technol. 287 (2016) 439.
[44] P.C. Nagajyothi, S.J. Cha, I.J. Yang, T.V.M. Sreekanth, K.J. Kim, H.M. Shin, J. Photochem. Photobiol. B: Biol. 146 (2015) 10.